Title: Ptbp1 is not required for retinal neurogenesis and cell fate specification.

Authors: Haley Appel[1], Rogger P. Carmen-Orozco[1], Clayton P. Santiago[1], Thanh Hoang[6-8], and Seth Blackshaw[1-5*].

Affiliations: [1]Solomon H. Snyder Department of Neuroscience, [2]Department of Ophthalmology, [3]Department of Neurology, [4]Institute for Cell Engineering, [5]Kavli Neuroscience Discovery Institute, Johns Hopkins University School of Medicine, Baltimore, MD, USA; [6]Department of Ophthalmology and Visual Sciences, [7]Department of Cell and Developmental Biology; [8]Michigan Neuroscience Institute, University of Michigan School of Medicine, Ann Arbor, MI 48105.
*to whom correspondence should be addressed at sblack@jhmi.edu.

Abstract: The RNA-binding protein Ptbp1 has been proposed as a master regulator of neuronal fate, repressing neurogenesis through its effects on alternative splicing and miRNA maturation. While prior studies using RNA interference suggested that Ptbp1 loss promotes neurogenesis, recent genetic studies have failed to replicate glia-to-neuron conversion following *Ptbp1* loss of function. To evaluate the role of Ptbp1 in developmental neurogenesis *in vivo*, we conditionally disrupted *Ptbp1* in retinal progenitors. Ptbp1 was robustly expressed in both retinal progenitors and Müller glia but absent from postmitotic neurons, and efficient loss of function in mutant animals was confirmed using immunostaining for Ptbp1. Furthermore, bulk RNA-Seq at E16 revealed accelerated expression of late-stage progenitor and photoreceptor-specific genes and altered splicing patterns in *Ptbp1* mutants, including increased inclusion of rod photoreceptor-specific exons. However, we observed no defects in retinal lamination, progenitor proliferation, or cell fate specification in mature retina. ScRNA-Seq of mature mutant retinas revealed only modest transcriptional changes which partially recapitulate alterations seen following selective deletion of *Ptbp1* in mature glia. Our findings demonstrate that Ptbp1 is dispensable for retinal cell fate specification and suggest that its proposed role as a central repressor of neurogenesis should be reevaluated.

Introduction: Control of neurogenesis in progenitor cells of the developing CNS involves an elaborate interplay between negative and positive regulators. Neurogenic bHLH factors such as Ascl1 and Neurog2 induce neural progenitors to undergo terminal neurogenic divisions, while inhibitory factors such as components of the Notch pathway and NFI family transcription factors promote proliferative divisions and gliogenesis (Clark et al., 2019; Hufnagel et al., 2013; Keeley et al., 2023; Lyu et al., 2021; Yaron et al., 2006). Studies in species such as zebrafish that undergo injury-induced neurogenesis by reprogramming of endogenous glial cells find that this process requires both upregulation of neurogenic factors and downregulation of inhibitory factors (Briona et al., 2015; Fausett et al., 2008; Lyu et al., 2023). This has recently inspired many studies aimed at inducing neurogenic competence in mammalian glia by selectively targeting these factors (Hoang et al., 2020; Jorstad et al., 2017; Le et al., 2025, 2024; Todd et al., 2022, 2021).

One factor that has attracted considerable interest is the RNA binding protein and splicing regulator Ptbp1, which is widely expressed in non-neuronal cells, including both neural progenitors and glia (Boutz et al., 2007; Lilleväli et al., 2001). It has been reported that Ptbp1 acts as a broad inhibitor of neuronal-specific splicing (Boutz et al., 2007; Ling et al., 2016), and inhibits maturation of miR-124a, which strongly promotes neurogenesis (Makeyev et al., 2007), while its paralog Ptbp2 promotes neuronal-specific splicing (Licatalosi et al., 2012; Li et al., 2014). It was also proposed that Ptbp1 acts as a master regulator of developmental neurogenesis in the CNS (Shibasaki et al., 2013). This then inspired studies which used *Ptbp1* knockdown to attempt to reprogram glia into functional neurons. While it was reported that *Ptbp1* knockdown *in vivo* induced robust generation of functional retinal ganglion cells from Müller glia (Zhou et al., 2020), as well as functional dopaminergic neurons from midbrain astrocytes (Qian et al., 2020), attempts to replicate these results by other groups were unsuccessful (Chen et al., 2022; Hoang et al., 2023, 2022; Wang et al., 2021; Xie et al., 2022). Notably, genetic loss of function of *Ptbp1* coupled with scRNA-Seq analysis failed to observe either loss of expression of glial-specific genes or induction of neuron-specific genes in mutant glia (Hoang et al., 2023, 2022).

This result raises questions about previous claims about the central role of Ptbp1 in controlling developmental neurogenesis. Previous functional studies of the role of Ptbp1 in neuronal development were primarily conducted *in vitro* using RNAi to interrogate Ptbp1 function (Linares et al., 2015; Spellman et al., 2007; Zheng et al., 2012). The few *in vivo* studies of Ptbp1 function in developing CNS have also almost exclusively used RNAi, and generally report modest and inconsistent phenotypes (Zhang et al., 2016). Conventional *Ptbp1* homozygous mutants are lethal, precluding direct analysis of its role in developmental neurogenesis (Shibayama et al., 2009). While one study reported accelerated cortical neurogenesis in *Ptbp1* heterozygotes (Shibasaki et al., 2013), these effects were also quite modest and difficult to interpret, given the broader role of Ptbp1 in early embryonic development.

The retina is a highly accessible and tractable model for the study of CNS neurogenesis and cell fate specification (Ptito et al., 2021), and conditional mutagenesis allows selective loss of function of any gene of interest in retinal progenitors without affecting viability (Sauer, 1998). We sought to use this approach to investigate the role of Ptbp1 in regulating neurogenesis and cell fate specification in developing retina. While we observe changes in RNA splicing and a moderate acceleration of retinal development as measured by bulk RNA-Seq, we do not observe any changes in proliferation or neurogenesis during retinal development, or changes in the cell type composition of *Ptbp1*-deficient retinas. Furthermore, we observe only modest changes in gene expression in adolescent mutant retina using scRNA-Seq analysis. These results demonstrate that *Ptbp1* is dispensable for retinal cell fate specification.

Results:

Ptbp1 mRNA is primarily expressed in retinal progenitors and Müller glia.

To examine the expression patterns of *Ptbp1* and *Ptbp2* in developing and adult neuroretina, we analyzed scRNA-Seq datasets from mouse and human retina that had been

previously generated by our lab (Clark et al., 2019; Lu et al., 2020). We observe high expression levels of *Ptbp1* mRNA in primary retinal progenitors in both species and Müller glia in mouse retina, with weaker expression in neurogenic progenitors, and little expression detectable in neurons at any developmental age. In contrast, *Ptbp2* is expressed in both progenitors and neurons, although with somewhat higher expression in retinal ganglion and amacrine cells (Fig. S1a). We observe that *Ptbp1* is expressed in primary progenitors at all developmental ages between E12 and P8 in mice and 9 and 20 gestational weeks in humans, although expression levels are moderately increased at later stages of neurogenesis (Fig. S1b).

$Chx10\text{-}Cre;Ptbp1^{lox/lox}$ mice show loss of Ptbp1 immunoreactivity in developing and mature retina.

To selectively disrupt *Ptbp1* function in retinal progenitors, we generated $Chx10\text{-}Cre;Ptbp1^{lox/lox}$ mice. In these mice, Cre recombinase is expressed broadly in retinal progenitors from the beginning of neurogenesis onwards (Rowan and Cepko, 2004), allowing efficient deletion of the conditional mutant allele of *Ptbp1* (Shibasaki et al., 2013) (Fig. 1a). In some cases, the *Sun1-GFP* reporter line was used to visualize patterns of Cre activity (Mo et al., 2015). Mutant mice were born at expected Mendelian ratios and showed no gross defects in retinal morphology. To confirm efficient deletion of *Ptbp1* in retinal progenitors, we performed immunohistochemistry for Ptbp1 at E14, P1, and P30 in both control $Chx10\text{-}Cre;Ptbp1^{+/l+}$ and homozygous mutant and $Chx10\text{-}Cre;Ptbp1^{lox/lox}$ and $Chx10\text{-}Cre;Ptbp1^{lox/lox}$*;Sun1-GFP mice* (Fig. 1b-d). Perinuclear Sun1-GFP expression was observed in all retinal cells in $Chx10\text{-}Cre;Ptbp1^{lox/lox}$*;Sun1-GFP mice*, reflecting the broad retinal progenitor-specific activity of the *Chx10-Cre* transgene, while nuclear GFP expression was observed in retinal progenitors (Mo et al., 2015), reflecting the fact that a Cre-GFP fusion is used in the *Chx10-Cre* transgenic line (Rowan and Cepko, 2004). At all stages, we observed a loss of *Ptbp1* protein expression in retinal progenitors and Müller glia, with a more than ten-fold reduction in the number of immunoreactive Müller glia observed at P30 (Fig. 1e). At both E14 and P1, we also observed a variable level of immunoreactivity in cells in the ganglion cell layer in control mice, which was also seen in $Chx10\text{-}Cre;Ptbp1^{lox/lox}$ mice, suggesting that this may represent crossreactivity with an unknown epitope. This ganglion cell layer staining was not observed at P30, however. This demonstrates that *Ptbp1* is efficiently and selectively deleted in retinal progenitors from early stages of neurogenesis.

Embryonic $Chx10\text{-}Cre;Ptbp1^{lox/lox}$ mice show shifts in temporal identity, increased expression of genes specific to photoreceptors, and altered patterns of RNA splicing.

To further investigate the effects of *Ptbp1* deletion on embryonic progenitors, we conducted bulk RNA-Seq on whole retina from E16 wildtype, $Chx10\text{-}Cre;Ptbp1^{lox/+}$, and $Chx10\text{-}Cre;Ptbp1^{lox/lox}$ retinas. A comparison of heterozygous $Chx10\text{-}Cre;Ptbp1^{lox/+}$ and homozygous $Chx10\text{-}Cre;Ptbp1^{lox/lox}$ mutants identified 2075 genes that were significantly differentially expressed (Fig. 2a, Extended Data 1). As expected, homozygotes showed a loss of *Ptbp1* expression along with a compensatory upregulation of *Ptbp2*, as has previously been observed following selective disruption of *Ptbp1* in mature Müller glia (Hoang et al., 2022) (Fig. 2b). In addition, we observed a modest increase in expression of multiple genes specific to both rods and cone photoreceptors – including *Opn1sw* and *Rcvrn* – as well as altered expression of

multiple genes selectively expressed in either early or late-stage RPCs (Clark et al., 2019; Lu et al., 2020; Lyu et al., 2021). For instance, the early-stage RPC-specific genes *Sfrp2* and *Foxp1* were downregulated, while late-stage RPC-enriched genes such as *Sox8*, *Nfix*, and *Hes5* were upregulated (Fig. 2b). Gene Ontology (GO) enrichment analysis likewise showed significant upregulation of genes involved in photoreceptor cell development and genes controlling synaptic function (Fig. 2c). However, immunohistochemical analysis does not detect any clear changes in the expression of HuC/D+NeuN, Otx2 or Opn1sw in *Chx10-Cre;Ptbp1*$^{lox/lox}$ homozygous mutants relative to *Chx10-Cre;Ptbp1*$^{+/+}$ control at either E14 or P0, and the number of Otx2-positive cells at P0 was not altered (Fig. S2). This implies that while at the transcriptional level retinal development in embryonic *Ptbp1* mutants appears to be moderately accelerated, based on higher expression of both markers of late-stage retinal progenitors and photoreceptors, this does not result in an increase in number of photoreceptors at this stage.

In light of the established role of Ptbp1 in regulating RNA splicing in non-neuronal cells, we analyzed splicing differences in *Ptbp1*-deficient retinas using our dataset. We identified 864 differential percent-spliced-in (PSI) events, including changes in retained introns, alternative 5′ or 3′ splice site usage, mutually exclusive exons, and exon skipping, consistent with the known role of Ptbp1 as a splicing repressor (Fig. 2d–e, Extended Data 1) (Vuong et al., 2016; Yap et al., 2012). To assess whether these splicing changes reflect neuronal or rod photoreceptor maturation, we compared our differential splicing events to those observed in adult neurons and rods (Ling et al., 2020). We found that 8 splicing events (7%) known to be enriched in central nervous system neurons and 19 events (35%) specific to rods overlapped with the splicing changes observed in *Ptbp1*-deficient retinas. (Fig. 2f, Extended Data 1).

Gene expression and splicing changes were compared across several reference tissues: heart tissue and Thy1-positive neurons, mature hair cells, microglia, and astrocytes (Fig. S3a,b). A heatmap of differentially expressed genes showed that while *Ptbp1*-deficient retinas diverged from WT retinas, their expression profiles did not resemble those of fully differentiated cell types like rods, astrocytes, or adult WT retina (Fig. S3c). Consistently, Pearson correlation analysis revealed that *Ptbp1*-deficient and WT retinas were more similar to each other than to fully differentiated neuronal or glial populations (Fig. S3d). Splicing profile analysis further revealed that while there was high correlation of PSI between *Ptbp1*-deficient and WT retinas, *Ptbp1*-deficient retinas more closely resembled Thy1-positive neurons, whereas WT retinas aligned more strongly with mature cells such as astrocytes, microglia, and auditory hair cells (Fig. S3e-f). Together, these results suggest that although *Ptbp1* loss of function induces hundreds of alternative splicing events, the magnitude of PSI changes in the KO retinas remains considerably lower than that seen in fully differentiated cell types (Extended Data 3). Thus, while a subset of splicing events overlaps with those characteristic of mature neurons or rods, the overall splicing and expression profiles of KO retinas are more similar to those of developing retinal tissue rather than terminally differentiated neuronal or glial populations.

Chx10-Cre;Ptbp1$^{lox/lox}$ mice show no changes in retinal progenitor proliferation or neurogenesis.

To determine whether retinal progenitor-specific loss of function of *Ptbp1* resulted in a depletion of retinal progenitors, we conducted EdU labeling to quantify the number of cells in S-phase in P0 retina (Fig. 3a). We did not observe any significant differences in the number of EdU-positive cells between Cre negative *Ptbp1*$^{lox/lox}$ controls and *Chx10-Cre;Ptbp1*$^{lox/lox}$ mice (Fig. 3b,c). To determine whether loss of function of *Ptbp1* influenced cell type specification in developing retina, we conducted immunostaining for a range of cell type-specific markers in *Chx10-Cre* control and *Chx10-Cre;Ptbp1*$^{lox/lox}$ mice (Fig. 4). Although Ptbp1 immunoreactivity was lost in homozygous mutant retinas (Fig. 4a), we did not observe any significant changes in the numbers of distribution of Sox9-positive Müller glia (Fig. 4b,f), HuC/D-positive amacrine and ganglion cells (Fig. 4c,f), Otx2-positive bipolar cells and photoreceptors (Fig. 4c,f), Rbpms-positive retinal ganglion cells (Fig. 4d,f), or cone arrestin-positive cone photoreceptors (Fig. 4e,f). Taken together, these findings show that *Ptbp1* loss of function induces neither precocious cell cycle exit nor affects normal levels and patterns of developmental neurogenesis and cell fate specification.

***Chx10-Cre;Ptbp1*$^{lox/lox}$ mice show only modest changes in gene expression in the mature retina.**

Despite the lack of any obvious defects in proliferation or cell fate specification in *Ptbp1*-deficient retinas, it nonetheless remained possible that this mutant might generate more subtle defects that are detectable using single-cell RNA-Seq analysis of whole retina. We therefore generated scRNA-Seq libraries from both P30 *Chx10-Cre;Ptbp1*$^{+/l+}$ and *Chx10-Cre;Ptbp1*$^{lox/lox}$ mice. No changes in the identity or composition of any retinal cell type were observed (Fig. 5a-c). The overall identities and proportions of major retinal cell types appeared broadly similar between control and knockout sample (Fig. 5a-c). A modest number of genes in rod and cone photoreceptors, as well as bipolar neurons, showed statistically significant changes in gene expression (Fig. S4, Extended Data 2). A subset of phototransduction (*Pde6g*, *Guca1a*, *Pdc*, *Rcvrn*), photoreceptor-specific structural components (*Rom1*), and rod-specific transcription factors *Nrl* and *Nr2e3*, all showed modest but significant increases in expression in rods, while transcription factors such as *Otx2* and *Prdm1*, which are more prominently expressed in immature photoreceptors, showed significantly reduced expression. Cone photoreceptors showed increased expression of some phototransduction components (*Pde6c*, *Rcvrn*, *Guca1a*) and decreased expression of others (*Arr3*).

The largest number of differentially-expressed genes were observed in Müller glia (Fig. 5d). Several of the most strongly upregulated genes – notably including *Ptbp2*, *Fxyd6*, *Mt1*, and *Mt3* – were previously found to be upregulated by selective loss of function of *Ptbp1* in mature Müller glia in *Glast-CreER;Ptbp1*$^{lox/lox}$ mice, with nearly a third of all significantly downregulated genes shared between both mutants (Hoang et al., 2022)(Fig. 5e, Extended Data 2). However, no significant changes in canonical markers of Müller glia such as *Sox9*, *Apoe*, *Glul*, or *Rlbp1* were observed (Fig. 5f).

Discussion:

Previous studies have reported that Ptbp1 acts in neural progenitors in the CNS as a master repressor of neuronal fate (Hu et al., 2018; Shibasaki et al., 2013). If this were the case,

we would expect that *Ptbp1* loss of function in early development would rapidly lead to precocious cell cycle exit and reduction in the number of progenitor cells. As a result, we would expect to observe an overrepresentation of early-born cell types such as retinal ganglion cells and cone photoreceptors at the expense of late-born cell types such as bipolar interneurons and, in particular, Müller glia. However, we observe that while Ptbp1 is robustly expressed in both retinal progenitors and mature glia, as in other CNS regions, loss of *Ptbp1* function in early-stage retinal progenitors does not induce any significant developmental defects. Despite efficient and widespread loss of Ptbp1 expression from E14 onwards, we do not observe any changes in progenitor proliferation, retinal cell type composition, or expression of canonical Müller glia marker genes in mature retina. The changes in gene expression that are observed in adolescent *Ptbp1*-deficient retinas are quite modest, although increased levels of several photoreceptor-specific genes are observed. This is consistent with previous studies showing that *Ptbp1* knockdown enhances photoreceptor-specific splicing of a subset of alternatively spliced genes (Ling et al., 2020), and implies that this may indirectly increase expression of a subset of rod-specific genes.

At E16, however, homozygous *Ptbp1* mutants do show changes in gene expression consistent with previously reported functions. These retinas show increased expression of *Ptbp2*, the neuronally-enriched paralog of *Ptbp1*, along with increased expression of genes specific to late-stage progenitors and photoreceptor precursors. Furthermore, *Ptbp1* mutants exhibit altered RNA splicing and inclusion of a subset of exons specific to rod photoreceptors. While this is apparently consistent with reports that developmental loss of *Ptbp1* function promotes neurogenesis by inducing a neuronal-like splicing pattern in neural progenitors (Boutz et al., 2007; Hu et al., 2018; Shibasaki et al., 2013; Vuong et al., 2016), this does not result in changes in either progenitor proliferation or any change in retinal cell type composition in either the developing or adolescent retina. This argues against the idea that *Ptbp1* loss simply accelerates the timing of neurogenesis, as there is no evidence for increased photoreceptor production or altered proliferation in embryonic or neonatal retina. An alternative interpretation would be that *Ptbp1* loss of function leads to the precocious formation of ectopic neurons which rapidly undergo cell death. Further studies will be needed to resolve this question.

Following closely behind studies that fail to show any role for Ptbp1 in regulating glia-to-neuron reprogramming in adult CNS (Chen et al., 2022; Hoang et al., 2023, 2022; Wang et al., 2021), these findings call into question previous models that place Ptbp1 in a central position in controlling developmental neurogenesis. The reason for this discrepancy is not entirely clear. Previous studies using knockdown may have been complicated by off-target effects (Jackson et al., 2003), and conditions for *in vitro* analysis may not have accurately replicated conditions in the native CNS. It is also possible that compensatory mechanisms differ between knockdown and knockout approaches. Notably, a recent study (Konar et al., 2025) reported that *Ptbp1* knockdown promotes Müller glia proliferation in zebrafish, suggesting that effects of acute reduction of *Ptbp1* mRNA may not fully mirror those of complete loss-of-function. Alternatively, upregulation of the widely expressed paralog *Ptbp2* may have compensated for developmental defects resulting from *Ptbp1* loss of function. Generation of conditional double mutant mice will be necessary to definitively exclude this possibility. Additionally, the use of *Chx10-Cre* in this

study does not exclude a potential role for *Ptbp1* during early stages of retinal development prior to E11, when the Cre is first expressed. Regardless, this study demonstrates that *Ptbp1* is dispensable for the process of retinal cell fate specification, and we anticipate that this will likely hold for other CNS regions.

Methods:

Mice

Mice were raised and housed in a climate-controlled pathogen-free facility on a 14/10 h light/dark cycle. Mice used in this study were *Chx10-Cre* (JAX #005105) *Ptbp1*$^{lox/lox}$ mice carrying loxP sites that flank the promoter and 1st exon of *Ptbp1* were generated as described previously (Shibayamaetal.,2009). *Chx10-Cre;Ptbp1*$^{lox/lox}$ mice were generated by crossing *Chx10-Cre* with conditional *Ptbp1*$^{lox/lox}$ mice. *Chx10-Cre;Ptbp1*$^{lox/lox}$;*Sun1-GFP* mice were also examined in some cases to visualize Cre activity in postmitotic neurons (Mo et al., 2015). Maintenance and experimental procedures performed on mice were in accordance ARRIVE guidelines for animal research, with the protocol approved by the Institutional Animal Care and Use Committee (IACUC) at the Johns Hopkins School of Medicine under protocol number MO22M22.

EdU treatment:

Chx10-Cre control and *Chx10-Cre;Ptbp1*$^{lox/lox}$ neonatal mice were administered EdU (Abcam, #ab146186) via subcutaneous injection at P0 [10-20 µl of 5 mg/ml in PBS]. Retinas were collected two hours post EdU injection for analysis.

Immunohistochemistry and imaging

Collection and immunohistochemical analysis of retinas were performed as described previously (Hoang et al., 2020). Briefly, mouse eye globes were fixed in 4% paraformaldehyde (ElectronMicroscopySciences, #15710) for 1 h at 4°C. Retinas were dissected in 1x PBS and incubated in 30% sucrose overnight at 4°C.

Retinas were then embedded in OCT (VWR, #95057-838), cryosectioned at 16 µm thickness, and stored at −20°C. Sections were dried for 30 min in a 37°C incubator and washed 3 x 5 min with 0.1% TritonX-100 in PBS (PBST). EdU labeling was performed by using Click-iT EdU kit (ThermoFisher, #C10340) following the manufacturer's instructions. Sections were then incubated in 10% Horse Serum (ThermoFisher, #26050070), 0.4% TritonX-100 in 1x PBS (blocking buffer) for 2 h at room temperature (RT) and then incubated with primary antibodies in the blocking buffer overnight at 4°C. Primary antibodies used in this study were: rabbit anti-Ptbp1 (1:200, Invitrogen, #PA3-81297), rabbit anti-Ptbp1 (1:200, ABclonal, #A6107), rabbit anti-RBPMS (1:200,Proteintech, #151871-AP), rabbit anti-cone arrestin (1:200, Millipore Sigma, #AB15282), goat anti-OTX2 (1:200, R&D Systems, #AF1979), mouse anti-HuC/D (1:200, ThermoFisher Scientific, #A21271), mouse anti-NeuN (1:200, SigmaAldrich, #MAB377), rabbit anti-SOX9 (1:200, SigmaAldrich, #AB5535) and chicken anti-GFP (1:400, ThermoFisher Scientific, #A10262). An equal mixture of anti-HuC/D and NeuN antibodies was used to detect amacrine and ganglion cells.

Sections were washed 3 x 5 min with PBST to remove excess primary antibodies and were incubated in secondary antibodies in blocking buffer for 2 h at RT. Sections were then counterstained with DAPI in PBST, washed 3 x 5 min in PBST and mounted with ProLong Gold Antifade Mountant (Invitrogen, #P36935) under coverslips (VWR, #,48404-453), air-dried, and stored at 4°C. Fluorescent images were captured using a Zeiss LSM 700 confocal microscope.

Cell quantification and statistical analysis

Ptbp1-positive, Sox9-positive, HuC/D/Neun-positive, Otx2-positive, Rbpms-positive, and ArrestinC-positive cells were counted in total from 300μM sections per retina. For cell proliferation quantification, EdU-positive cells were counted from 300μM sections per retina. Each data point in the bar graphs was calculated from an individual retina. All cell quantification data were graphed and analyzed using GraphPad Prism 10. Multiple unpaired *t* tests or Mann-Whitney tests were used for analysis between samples of multiple groups. In all tests, values of $p < 0.05$ were considered to indicate significance.

Retinal cell dissociation

Briefly, one female mouse per genotype was euthanized by CO2. Retinas were dissected in fresh ice-cold PBS and retinal cells were dissociated using Papain Dissociation System (LK003150,Worthington). Dissociated cells were resuspended in ice-cold HBAG buffer containing 9.8mL HibernateA (BrainBits, #HALF500), 200mL B27 (ThermoFisher, #17504044), 20mL GlutaMAX (ThermoFisher, #35050061) and 0.5U/mL RNAse inhibitor. Cells were filtered through a 50mm filter. Cell count and viability were determined by using 0.4% Trypan blue.

Bulk RNA-sequencing library preparation

Retinas were dissected from E16 mice embryos and stored at -80C. Frozen retinal tissue was pooled into 7 samples by genotype: wildtype (WT (6 pooled retinas)); heterozygous *Ptbp1* mutant *Chx10-Cre;Ptbp1*$^{lox/+}$ (Het1 (5 pooled retinas), Het2 (5 pooled retinas), Het3 (6 pooled retinas)); and homozygous *Ptbp1* mutant ((KO1 (4 pooled retinas), KO2 (4 pooled retinas), and KO3 (6 pooled retinas)). RNA was extracted using the RNeasy Micro Plus kit (Qiagen). Illumina Stranded mRNA Prep Ligation kit was used for bulk RNA library preparation. Libraries were sequenced on the Illumina NovaSeq X.

Single-cell RNA-sequencing (scRNA-seq) library preparation

scRNA-seq were prepared on dissociated retinal cells using the 10X Genomics Chromium Single Cell 3' Reagents Kit v3.1 (10X Genomics, Pleasanton, CA). Libraries were constructed following the manufacturer's instructions and were sequenced using the Illumina NovaSeq 6000. The sequencing data were aligned to the mm10 reference genome and a cell-by-gene matrix was generated using the Cell Ranger 7.0.1 pipeline (10X Genomics).

ScRNA-seq data analysis

ScRNA-seq of control *Chx10-Cre;Ptbp1*$^{+/+}$ and homozygous mutant *Chx10-Cre;Ptbp1*$^{lox/lox}$ mice were analyzed using the Seurat package (Hao et al., 2021). Briefly, cells were filtered to retain those with more than 200 and fewer than 5,000 detected genes, more than 700 and fewer than

10,000 total transcripts, and less than 20% mitochondrial gene content. The data were normalized using the default log-normalization parameters, the top 4000 highly variable features were identified, and data were scaled while regressing out mitochondrial gene content. Principal component analysis (PCA) was then performed on the variable genes followed by louvain clustering and UMAP visualization using the top 12 principal components. Expression of key marker genes within each cell cluster were used to confirm the appropriate assignment of cell types. Differentially expressed genes between groups were determined using the Wilcoxon rank sum test. The clusterProfiler R package was used to perform gene ontology enrichment analysis of biological processes found in the differentially expressed gene lists (Yu et al., 2012).

Bulk RNA-seq analysis

Reads were processed using the rMATS-turbo pipeline (Wang et al., 2024), which performs alignment with STAR and custom splice junction counts. Alignments were generated using the GRCm38 mouse genome (Release M10) with GENCODE annotation. Gene-level counts were then extracted from the resulting BAM files using featureCounts, and differential gene expression was analyzed with the DESeq2 package in R (Liao et al., 2014; Love et al., 2014). Comparisons between *Ptbp1* heterozygous (Het) and knockout (KO) samples identified differentially expressed genes based on an absolute log2 fold change greater than 0.263 (representing at least a 20% change in expression) and an adjusted p-value below 0.05. We incorporated publicly available bulk RNA-seq datasets for comparative analysis, including embryonic day 16 retina (E16: GSM2720095, GSM2720096), postnatal day 28 retina (P28: GSM2720111, GSM2720112), Thy1-positive neurons (GSM2392791), astrocytes (GSM1269903, GSM1269904, microglia (GSM1269913, GSM1269914), hair cells (GSM1602228, GSM1602229), and heart tissue (GSM1223635) (Brooks et al., 2019; Cai et al., 2015; Giudice et al., 2014; Yang et al., 2017; Zhang et al., 2014). Hair cells and heart tissue samples were chosen as examples of high and low Ptbp1 expression, respectively, based on data from ASCOT (Ling et al., 2020). We generated a Pearson correlation matrix to assess overall sample similarity. Splicing differences were evaluated using filtered rMATS output, applying the following thresholds: read coverage ≥ 15, minimum PSI = 0.05, maximum PSI = 0.95, significant FDR (sigFDR) ≤ 0.05, |ΔPSI| ≥ 0.10, background FDR (bgFDR) ≤ 0.5, and background within-group ΔPSI ≤ 0.2. For the E16 and P28 retina datasets, we used more relaxed filters (read coverage ≥ 0, PSI between 0.01 and 0.99) to ensure inclusion of lower-abundance events. Splicing events specific to rods and various neuronal subtypes were queried from the ASCOT supplementary files and visually inspected using the UCSC Genome Browser to assess their presence in bulk RNA-seq datasets. This analysis followed the approach described in previous studies (Carmen-Orozco et al., 2024; Ling et al., 2020).

Data availability: All raw RNA-Seq and scRNA-Seq data are publicly available through the Gene Expression Omnibus under accession numbers GSE300588 and GSE300607. Analysis scripts used in this study are accessible at: https://github.com/csanti88/ptbp1_2025. Bulk RNA-seq and other tissue track plots visualizations are available at: https://genome.ucsc.edu/s/roggercarmen/Ptbp1KO_Retina

Acknowledgements: This work was supported by NIH grant R01EY036173 to S.B.

Declaration of Interests: S.B. is a cofounder, shareholder, and scientific advisory board member of CDI Labs LLC, and receives research support from Genentech.

Figure legends:

Figure 1. *Ptbp1* is successfully deleted in *Chx10-Cre;Ptbp1$^{lox/lox}$* mice in developing and mature retina.
(A) A schematic diagram of the generation of specific deletion of *Ptbp1* in early RPCs using *Chx10-Cre*. **(B)** Representative immunostaining for *Ptbp1* expression in *Chx10-Cre;Ptbp1$^{+/+}$* (Ptbp1-Ctrl) and *Chx10-Cre;Ptbp1$^{lox/lox}$* (Ptbp1-KO) mice at E14.5, **(C)** *Chx10-Cre;Ptbp1$^{+/+}$;Sun1-GFP* and *Chx10-Cre;Ptbp1$^{lox/lox}$;Sun1-GFP* mice at P1, **(D)** and *Chx10-Cre;Ptbp1$^{+/+}$* and *Chx10-Cre;Ptbp1$^{lox/lox}$;Sun1-GFP* mice P30. **(E)** Quantification of Ptbp1-positive cells in Ptbp1-Ctrl and Ptbp1-KO retinas (n=8/genotype). Significance was determined via unpaired *t* test: **** p<0.0001. Each data point was calculated from an individual retina. ONL, outer nuclear layer; INL, inner nuclear layer; GCL, ganglion cell layer. Scale bar= 100 µm.

Figure 2. BulkRNA-seq analysis reveals accelerated differentiation and altered RNA splicing in *Chx10-Cre;Ptbp1$^{lox/lox}$* mice at E16.5.
(A) Volcano plot showing 2075 differentially expressed genes between heterozygous *Chx10-Cre;Ptbp1$^{lox/+}$* and homozygous *Chx10-Cre;Ptbp1$^{lox/lox}$* mutants as measured by bulk RNA-seq. **(B)** Heatmap of select differentially expressed genes in wildtype *Chx10-Cre;Ptbp1$^{+/+}$*, heterozygous *Chx10-Cre;Ptbp1$^{lox/+}$*, and homozygous *Chx10-Cre;Ptbp1$^{lox/lox}$* samples. **(C)** Gene set enrichment analysis showing activated and repressed gene ontology terms in the homozygous *Ptbp1* mutant samples. **(D)** Barplot showing 864 splicing changes in homozygous *Ptbp1* mutant samples by splicing class including retained-introns (54 events), alternative 5' splice site (32 events), alternative 3' splice site (67 events), mutually-exclusive exons (128 events) and skipped-exons (583 events). **(E)** Track plots showing examples of alternative splicing of exons (arrows) in the *Ptbp1* mutant samples. **(F)** Bar plot showing that **7%** of neuron-enriched and **35%** of rod-specific splicing events overlap with splicing changes observed in *Ptbp1* mutants.

Figure 3. *Ptbp1* deletion does not alter retinal progenitor proliferation.
(A) A schematic diagram of the experimental timeline for labeling dividing cells using EdU. **(B)** Representative immunostaining for Ptbp1 expression and EdU labeling in Ptbp1-Ctrl and Ptbp1-KO mice at P0. **(C)** Quantification of EdU-positive cells in Ptbp1-Ctrl and Ptbp1-KO retinas (n≥2/genotype). Significance was determined via Mann-Whitney test: ns=p>0.05. Each data point was calculated from an individual retina. ONL, outer nuclear layer; INL, inner nuclear layer; GCL, ganglion cell layer. Scale bar=100 µm.

Figure 4. *Ptbp1* deletion does not alter retinal neurogenesis.
(A) Representative immunostaining for Ptbp1, **(B)** Sox9, **(C)** HuC/D+NeuN, Otx2, **(D)** Rbpms, and **(E)** Cone-arrestin in Ptbp1-Ctrl and Ptbp1-KO mice at P30. **(F)** Quantification of Sox9, HuC/D/NeuN, Otx2, Rbpms, and Cone-arrestin-positive cells in Ptbp1-Ctrl and Ptbp1-KO retinas

(n≥4/genotype). Significance was determined via multiple unpaired *t* tests: ns=p>0.05. Each data point was calculated from an individual retina. ONL, outer nuclear layer; INL, inner nuclear layer; GCL, ganglion cell layer. Scale bar= 100 µm.

Figure 5. ScRNA-seq analysis reveals modest transcriptional changes in Müller glial gene expression in *Chx10-Cre;Ptbp1$^{lox/lox}$* mice. (A) Uniform manifold approximation and projection (UMAP) plots showing cell types captured in the *Chx10-Cre;Ptbp1$^{+/+}$* (Ptbp1-Ctrl) and *Chx10-Cre;Ptbp1$^{lox/lox}$* **(**Ptbp1-KO) merged dataset. **(B)** UMAP plots showing cell types separated by genotype with the percentage of Müller glia in each group. **(C)** Barplot showing cell proportions for each cell type in both genotypes. **(D)** Volcano plot showing differentially expressed genes in Müller glia between Ptbp1-Ctrl and Ptbp1-KO samples. **(E)** Venn diagram comparison of upregulated and downregulated differentially expressed genes for Müller glia between this dataset and previously published data analyzing Müller glia-specific loss of function of *Ptbp1* (Hoang et al., 2022). **(F)** Violin plot showing no significant changes in the expression of canonical Müller glia markers in Ptbp1-KO sample compared to Ptbp1-Ctrl.

Figure S1. Cellular expression patterns of *Ptbp1* and *Ptbp2* during mouse and human retinal development. (A) 3D UMAP plot showing cell types from combined timepoints (E14-Adult) of mouse retinal development utilizing publicly available data from (Clark et al., 2019). **(B)** Gene plots for *Ptbp1* and *Ptbp2* expression during mouse retinal development. **(C)** Heatmaps of *Ptbp1* and *Ptbp2* expression patterns in RPCs at varying time points during mouse retinal development. **(D)** Heatmaps of *Ptbp1* and *Ptbp2* expression patterns in different mouse retinal cell types. **(E)** 3D UMAP plot showing cell types from combined timepoints (Hgw9-Adult) of human retinal development utilizing publicly available data from (Lu et al., 2020). **(F)** Gene plots for *Ptbp1* and *Ptbp2* expression during human retinal development. **(G)** Heatmaps of *Ptbp1* and *Ptbp2* expression patterns in RPCs at varying time points during human retinal development. **(H)** Heatmaps of *Ptbp1* and *Ptbp2* expression patterns in different human retinal cell types.

Figure S2. Immunostaining does not detect changes in cell composition in E14 or P0 *Ptbp1*-deficient retina.
(A) Representative immunostaining for, HuC/D+NeuN and **(B)** Otx2 in Ptbp1-Ctrl and Ptbp1-KO mice at E14. **(C)** Representative immunostaining for Opn1sw and **(D)** Otx2 in Ptbp1-Ctrl and Ptbp1-KO mice at P0, with the Ptbp1-KO mouse having the *Chx10-Cre;Ptbp1$^{lox/lox}$;Sun1-GFP* genotype (Mo et al., 2015). Note that GFP signal is found in all retinal cell types, since the Cre transgene is active in retinal progenitors over the full course of neurogenesis. **(E)** Quantification of Otx2-positive cells in Ptbp1-Ctrl and Ptbp1-KO retinas at P0 (n≥4/genotype). Significance was determined via Mann-Whitney test: ns=p>0.05. Each data point was calculated from an individual retina. ONL, outer nuclear layer; INL, inner nuclear layer; GCL, ganglion cell layer. Scale bar= 100 µm.

Figure S3. BulkRNA-seq analysis reveals altered gene expression and splicing patterns in E16 *Chx10-Cre;Ptbp1$^{lox/lox}$* mice retina.
(A) Bar charts showing *Ptbp1* and **(B)** *Ptbp2* expression in various cell types and tissues using the ASCOT browser (Ling et al., 2020). Highlighted samples are rods photoreceptors at P2,

heart tissue showing low *Ptbp1* expression and cochlear hair cells showing high *Ptbp1* expression. **(C)** Heatmap of select differentially expressed genes between individual replicates samples for wildtype (WT), heterozygous *Chx10-Cre;Ptbp1*$^{lox/+}$ (Het1, Het2, Het3), and homozygous *Chx10-Cre;Ptbp1*$^{lox/lox}$ (KO1, KO2, KO3) *Ptbp1* mutant retinal samples analyzed in this study, along with publicly available bulk RNA-seq datasets including embryonic day 16 retina, postnatal day 28 retina, Thy1-positive neurons, astrocytes, microglia, hair cells and heart tissue. **(D)** Pearson correlation plot for identified differentially expressed genes between Het and KO samples, plotted across all samples including publically available datasets used. **(E)** Heatmap showing PSI values and **(F)** pearson correlation plot for splicing events identified as differentially spliced between Het and KO samples, plotted across all samples including publicly available datasets.

Figure S4. ScRNA-seq analysis identifies differentially expressed genes in major adolescent retinal cell types following developmental loss of function of *Ptbp1*.
(A) Dot Plot of cell type-specific markers used to identify clusters for each major retinal cell type. **(B)** Volcano plot showing differentially expressed genes for bipolar cells (BC), **(C)** amacrine cells (AC), **(D)** rod photoreceptors and **(E)** cone photoreceptors between Ptbp1-Ctrl and Ptbp1-KO samples.

Extended Data:

Extended Data 1. Bulk RNA-Seq analysis.
Table of 2075 differentially expressed genes between heterozygous *Chx10-Cre;Ptbp1*$^{lox/l+}$ and homozygous *Chx10-Cre;Ptbp1*$^{lox/lox}$ mutants identified by bulk RNA-Seq at E16.5, table of 864 differential splicing changes, and table of adult neuronal and rod enriched splicing events that overlap with the differential splicing events in the bulk RNA-Seq dataset.

Extended Data 2. scRNA-Seq analysis.
Proportions of cell types in the Ptbp1-Ctrl and Ptbp1-KO scRNA-Seq datasets. Table of differentially expressed genes between *Chx10-Cre;Ptbp1*$^{+/+}$ control and homozygous *Chx10-Cre;Ptbp1*$^{lox/lox}$ mutants identified by scRNA-Seq in adolescent retina for Müller glia (496), bipolar cells (433), amacrine cells (138), rod photoreceptor (345) and cone photoreceptor cells (74) with adjusted p-value of 0.05. Positive avg_log2FC scores represent upregulated genes within the Ptbp1-KO sample.

Extended Data 3. Bulk RNA-Seq analysis of Rod and Neuron-specific exons.
Genome-browser view showing exon-level read coverage for 18 Rod-specific **(A)** and 8 Neuron-specific **(B)** exons across WT, heterozygous *Chx10-Cre;Ptbp1*$^{lox/l+}$ and homozygous *Chx10-Cre;Ptbp1*$^{lox/lox}$ mutant retinas and additional tissue including brain, rod photoreceptors (P2, P6, P14, P28), and various neuronal and glial cell types. Tracks indicate RNA-seq read density aligned to the mm10 genome, highlighting exon-specific differences in expression and potential alternative splicing events across genotypes.

References:

Boutz PL, Stoilov P, Li Q, Lin C-H, Chawla G, Ostrow K, Shiue L, Ares M Jr, Black DL. 2007. A post-transcriptional regulatory switch in polypyrimidine tract-binding proteins reprograms alternative splicing in developing neurons. *Genes Dev* **21**:1636–1652.
Briona LK, Poulain FE, Mosimann C, Dorsky RI. 2015. Wnt/ß-catenin signaling is required for radial glial neurogenesis following spinal cord injury. *Dev Biol* **403**:15–21.
Brooks MJ, Chen HY, Kelley RA, Mondal AK, Nagashima K, De Val N, Li T, Chaitankar V, Swaroop A. 2019. Improved Retinal Organoid Differentiation by Modulating Signaling Pathways Revealed by Comparative Transcriptome Analyses with Development In Vivo. *Stem Cell Reports* **13**:891–905.
Cai T, Jen H-I, Kang H, Klisch TJ, Zoghbi HY, Groves AK. 2015. Characterization of the transcriptome of nascent hair cells and identification of direct targets of the Atoh1 transcription factor. *J Neurosci* **35**:5870–5883.
Carmen-Orozco RP, Tsao W, Ye Y, Sinha IR, Chang K, Trinh VT, Chung W, Bowden K, Troncoso JC, Blackshaw S, Hayes LR, Sun S, Wong PC, Ling JP. 2024. Elevated nuclear TDP-43 induces constitutive exon skipping. *Mol Neurodegener* **19**:45.
Chen W, Zheng Q, Huang Q, Ma S, Li M. 2022. Repressing PTBP1 fails to convert reactive astrocytes to dopaminergic neurons in a 6-hydroxydopamine mouse model of Parkinson's disease. *Elife* **11**. doi:10.7554/eLife.75636
Clark BS, Stein-O'Brien GL, Shiau F, Cannon GH, Davis-Marcisak E, Sherman T, Santiago CP, Hoang TV, Rajaii F, James-Esposito RE, Gronostajski RM, Fertig EJ, Goff LA, Blackshaw S. 2019. Single-Cell RNA-Seq Analysis of Retinal Development Identifies NFI Factors as Regulating Mitotic Exit and Late-Born Cell Specification. *Neuron* **102**:1111–1126.e5.
Fausett BV, Gumerson JD, Goldman D. 2008. The proneural basic helix-loop-helix gene ascl1a is required for retina regeneration. *J Neurosci* **28**:1109–1117.
Giudice J, Xia Z, Wang ET, Scavuzzo MA, Ward AJ, Kalsotra A, Wang W, Wehrens XHT, Burge CB, Li W, Cooper TA. 2014. Alternative splicing regulates vesicular trafficking genes in cardiomyocytes during postnatal heart development. *Nat Commun* **5**:3603.
Hao Y, Hao S, Andersen-Nissen E, Mauck WM 3rd, Zheng S, Butler A, Lee MJ, Wilk AJ, Darby C, Zager M, Hoffman P, Stoeckius M, Papalexi E, Mimitou EP, Jain J, Srivastava A, Stuart T, Fleming LM, Yeung B, Rogers AJ, McElrath JM, Blish CA, Gottardo R, Smibert P, Satija R. 2021. Integrated analysis of multimodal single-cell data. *Cell* **184**:3573–3587.e29.
Hoang T, Kim DW, Appel H, Ozawa M, Zheng S, Kim J, Blackshaw S. 2023. Ptbp1 deletion does not induce astrocyte-to-neuron conversion. *Nature* **618**:E1–E7.
Hoang T, Kim DW, Appel H, Pannullo NA, Leavey P, Ozawa M, Zheng S, Yu M, Peachey NS, Blackshaw S. 2022. Genetic loss of function of Ptbp1 does not induce glia-to-neuron conversion in retina. *Cell Rep* **39**:110849.
Hoang T, Wang J, Boyd P, Wang F, Santiago C, Jiang L, Yoo S, Lahne M, Todd LJ, Jia M, Saez C, Keuthan C, Palazzo I, Squires N, Campbell WA, Rajaii F, Parayil T, Trinh V, Kim DW, Wang G, Campbell LJ, Ash J, Fischer AJ, Hyde DR, Qian J, Blackshaw S. 2020. Gene regulatory networks controlling vertebrate retinal regeneration. *Science* **370**. doi:10.1126/science.abb8598
Hufnagel RB, Riesenberg AN, Quinn M, Brzezinski JA 4th, Glaser T, Brown NL. 2013. Heterochronic misexpression of Ascl1 in the Atoh7 retinal cell lineage blocks cell cycle exit. *Mol Cell Neurosci* **54**:108–120.
Hu J, Qian H, Xue Y, Fu X-D. 2018. PTB/nPTB: master regulators of neuronal fate in mammals. *Biophys Rep* **4**:204–214.
Jackson AL, Bartz SR, Schelter J, Kobayashi SV, Burchard J, Mao M, Li B, Cavet G, Linsley PS. 2003. Expression profiling reveals off-target gene regulation by RNAi. *Nat Biotechnol* **21**:635–637.
Jorstad NL, Wilken MS, Grimes WN, Wohl SG, VandenBosch LS, Yoshimatsu T, Wong RO, Rieke F, Reh TA. 2017. Stimulation of functional neuronal regeneration from Müller glia in

adult mice. *Nature* **548**:103–107.
Keeley PW, Patel PS, Ryu MS, Reese BE. 2023. Neurog2 regulates Isl1 to modulate horizontal cell number. *Development* **150**. doi:10.1242/dev.201315
Konar GJ, Lingan AL, Vallone KT, Nguyen TD, Flickinger ZR, Patton JG. 2025. Depletion of Polypyrimidine tract binding protein 1 (ptbp1) activates Müller glia-derived proliferation during zebrafish retina regeneration via modulation of the senescence secretome. *Exp Eye Res* **257**:110420.
Le N, Awad S, Palazzo I, Hoang T, Blackshaw S. 2025. Viral-mediated Pou5f1 (Oct4) overexpression and inhibition of Notch signaling synergistically induce neurogenic competence in mammalian Müller glia. *Elife* **14**. doi:10.7554/eLife.106450
Le N, Vu T-D, Palazzo I, Pulya R, Kim Y, Blackshaw S, Hoang T. 2024. Robust reprogramming of glia into neurons by inhibition of Notch signaling and nuclear factor I (NFI) factors in adult mammalian retina. *Sci Adv* **10**:eadn2091.
Liao Y, Smyth GK, Shi W. 2014. featureCounts: an efficient general purpose program for assigning sequence reads to genomic features. *Bioinformatics* **30**:923–930.
Licatalosi DD, Yano M, Fak JJ, Mele A, Grabinski SE, Zhang C, Darnell RB. 2012. Ptbp2 represses adult-specific splicing to regulate the generation of neuronal precursors in the embryonic brain. *Genes Dev* **26**:1626–1642.
Lilleväli K, Kulla A, Ord T. 2001. Comparative expression analysis of the genes encoding polypyrimidine tract binding protein (PTB) and its neural homologue (brPTB) in prenatal and postnatal mouse brain. *Mech Dev* **101**:217–220.
Linares AJ, Lin C-H, Damianov A, Adams KL, Novitch BG, Black DL. 2015. The splicing regulator PTBP1 controls the activity of the transcription factor Pbx1 during neuronal differentiation. *Elife* **4**:e09268.
Ling JP, Chhabra R, Merran JD, Schaughency PM, Wheelan SJ, Corden JL, Wong PC. 2016. PTBP1 and PTBP2 Repress Nonconserved Cryptic Exons. *Cell Rep* **17**:104–113.
Ling JP, Wilks C, Charles R, Leavey PJ, Ghosh D, Jiang L, Santiago CP, Pang B, Venkataraman A, Clark BS, Nellore A, Langmead B, Blackshaw S. 2020. ASCOT identifies key regulators of neuronal subtype-specific splicing. *Nat Commun* **11**:137.
Li Q, Zheng S, Han A, Lin C-H, Stoilov P, Fu X-D, Black DL. 2014. The splicing regulator PTBP2 controls a program of embryonic splicing required for neuronal maturation. *Elife* **3**:e01201.
Love MI, Huber W, Anders S. 2014. Moderated estimation of fold change and dispersion for RNA-seq data with DESeq2. *Genome Biol* **15**:550.
Lu Y, Shiau F, Yi W, Lu S, Wu Q, Pearson JD, Kallman A, Zhong S, Hoang T, Zuo Z, Zhao F, Zhang M, Tsai N, Zhuo Y, He S, Zhang J, Stein-O'Brien GL, Sherman TD, Duan X, Fertig EJ, Goff LA, Zack DJ, Handa JT, Xue T, Bremner R, Blackshaw S, Wang X, Clark BS. 2020. Single-Cell Analysis of Human Retina Identifies Evolutionarily Conserved and Species-Specific Mechanisms Controlling Development. *Dev Cell* **53**:473–491.e9.
Lyu P, Hoang T, Santiago CP, Thomas ED, Timms AE, Appel H, Gimmen M, Le N, Jiang L, Kim DW, Chen S, Espinoza DF, Telger AE, Weir K, Clark BS, Cherry TJ, Qian J, Blackshaw S. 2021. Gene regulatory networks controlling temporal patterning, neurogenesis, and cell-fate specification in mammalian retina. *Cell Rep* **37**:109994.
Lyu P, Iribarne M, Serjanov D, Zhai Y, Hoang T, Campbell LJ, Boyd P, Palazzo I, Nagashima M, Silva NJ, Hitchcock PF, Qian J, Hyde DR, Blackshaw S. 2023. Common and divergent gene regulatory networks control injury-induced and developmental neurogenesis in zebrafish retina. *Nat Commun* **14**:8477.
Makeyev EV, Zhang J, Carrasco MA, Maniatis T. 2007. The MicroRNA miR-124 promotes neuronal differentiation by triggering brain-specific alternative pre-mRNA splicing. *Mol Cell* **27**:435–448.
Mo A, Mukamel EA, Davis FP, Luo C, Henry GL, Picard S, Urich MA, Nery JR, Sejnowski TJ,

Lister R, Eddy SR, Ecker JR, Nathans J. 2015. Epigenomic Signatures of Neuronal Diversity in the Mammalian Brain. *Neuron* **86**:1369–1384.
Ptito M, Bleau M, Bouskila J. 2021. The Retina: A Window into the Brain. *Cells* **10**:3269.
Qian H, Kang X, Hu J, Zhang D, Liang Z, Meng F, Zhang X, Xue Y, Maimon R, Dowdy SF, Devaraj NK, Zhou Z, Mobley WC, Cleveland DW, Fu X-D. 2020. Author Correction: Reversing a model of Parkinson's disease with in situ converted nigral neurons. *Nature* **584**:E17.
Rowan S, Cepko CL. 2004. Genetic analysis of the homeodomain transcription factor Chx10 in the retina using a novel multifunctional BAC transgenic mouse reporter. *Dev Biol* **271**:388–402.
Sauer B. 1998. Inducible Gene Targeting in Mice Using the Cre/loxSystem. *Methods* **14**:381–392.
Shibasaki T, Tokunaga A, Sakamoto R, Sagara H, Noguchi S, Sasaoka T, Yoshida N. 2013. PTB deficiency causes the loss of adherens junctions in the dorsal telencephalon and leads to lethal hydrocephalus. *Cereb Cortex* **23**:1824–1835.
Shibayama M, Ohno S, Osaka T, Sakamoto R, Tokunaga A, Nakatake Y, Sato M, Yoshida N. 2009. Polypyrimidine tract-binding protein is essential for early mouse development and embryonic stem cell proliferation. *FEBS J* **276**:6658–6668.
Spellman R, Llorian M, Smith CWJ. 2007. Crossregulation and functional redundancy between the splicing regulator PTB and its paralogs nPTB and ROD1. *Mol Cell* **27**:420–434.
Todd L, Hooper MJ, Haugan AK, Finkbeiner C, Jorstad N, Radulovich N, Wong CK, Donaldson PC, Jenkins W, Chen Q, Rieke F, Reh TA. 2021. Efficient stimulation of retinal regeneration from Müller glia in adult mice using combinations of proneural bHLH transcription factors. *Cell Rep* **37**:109857.
Todd L, Jenkins W, Finkbeiner C, Hooper MJ, Donaldson PC, Pavlou M, Wohlschlegel J, Ingram N, Mu X, Rieke F, Reh TA. 2022. Reprogramming Müller glia to regenerate ganglion-like cells in adult mouse retina with developmental transcription factors. *Sci Adv* **8**:eabq7219.
Vuong JK, Lin C-H, Zhang M, Chen L, Black DL, Zheng S. 2016. PTBP1 and PTBP2 Serve Both Specific and Redundant Functions in Neuronal Pre-mRNA Splicing. *Cell Rep* **17**:2766–2775.
Wang L-L, Serrano C, Zhong X, Ma S, Zou Y, Zhang C-L. 2021. Revisiting astrocyte to neuron conversion with lineage tracing in vivo. *Cell* **184**:5465–5481.e16.
Wang Y, Xie Z, Kutschera E, Adams JI, Kadash-Edmondson KE, Xing Y. 2024. rMATS-turbo: an efficient and flexible computational tool for alternative splicing analysis of large-scale RNA-seq data. *Nat Protoc* **19**:1083–1104.
Xie Y, Zhou J, Chen B. 2022. Critical examination of Ptbp1-mediated glia-to-neuron conversion in the mouse retina. *Cell Rep* **39**:110960.
Yang J, Liu A-Y, Tang B, Luo D, Lai Y-J, Zhu B-L, Wang X-F, Yan Z, Chen G-J. 2017. Chronic nicotine differentially affects murine transcriptome profiling in isolated cortical interneurons and pyramidal neurons. *BMC Genomics* **18**:194.
Yap K, Lim ZQ, Khandelia P, Friedman B, Makeyev EV. 2012. Coordinated regulation of neuronal mRNA steady-state levels through developmentally controlled intron retention. *Genes Dev* **26**:1209–1223.
Yaron O, Farhy C, Marquardt T, Applebury M, Ashery-Padan R. 2006. Notch1 functions to suppress cone-photoreceptor fate specification in the developing mouse retina. *Development* **133**:1367–1378.
Yu G, Wang L-G, Han Y, He Q-Y. 2012. clusterProfiler: an R package for comparing biological themes among gene clusters. *OMICS* **16**:284–287.
Zhang X, Chen MH, Wu X, Kodani A, Fan J, Doan R, Ozawa M, Ma J, Yoshida N, Reiter JF, Black DL, Kharchenko PV, Sharp PA, Walsh CA. 2016. Cell-Type-Specific Alternative

Splicing Governs Cell Fate in the Developing Cerebral Cortex. *Cell* **166**:1147–1162.e15.
Zhang Y, Chen K, Sloan SA, Bennett ML, Scholze AR, O'Keeffe S, Phatnani HP, Guarnieri P, Caneda C, Ruderisch N, Deng S, Liddelow SA, Zhang C, Daneman R, Maniatis T, Barres BA, Wu JQ. 2014. An RNA-sequencing transcriptome and splicing database of glia, neurons, and vascular cells of the cerebral cortex. *J Neurosci* **34**:11929–11947.
Zheng S, Gray EE, Chawla G, Porse BT, O'Dell TJ, Black DL. 2012. PSD-95 is post-transcriptionally repressed during early neural development by PTBP1 and PTBP2. *Nat Neurosci* **15**:381–8, S1.
Zhou H, Su J, Hu X, Zhou C, Li H, Chen Z, Xiao Q, Wang B, Wu W, Sun Y, Zhou Y, Tang C, Liu F, Wang L, Feng C, Liu M, Li S, Zhang Y, Xu H, Yao H, Shi L, Yang H. 2020. Glia-to-Neuron Conversion by CRISPR-CasRx Alleviates Symptoms of Neurological Disease in Mice. *Cell* **181**:590–603.e16.

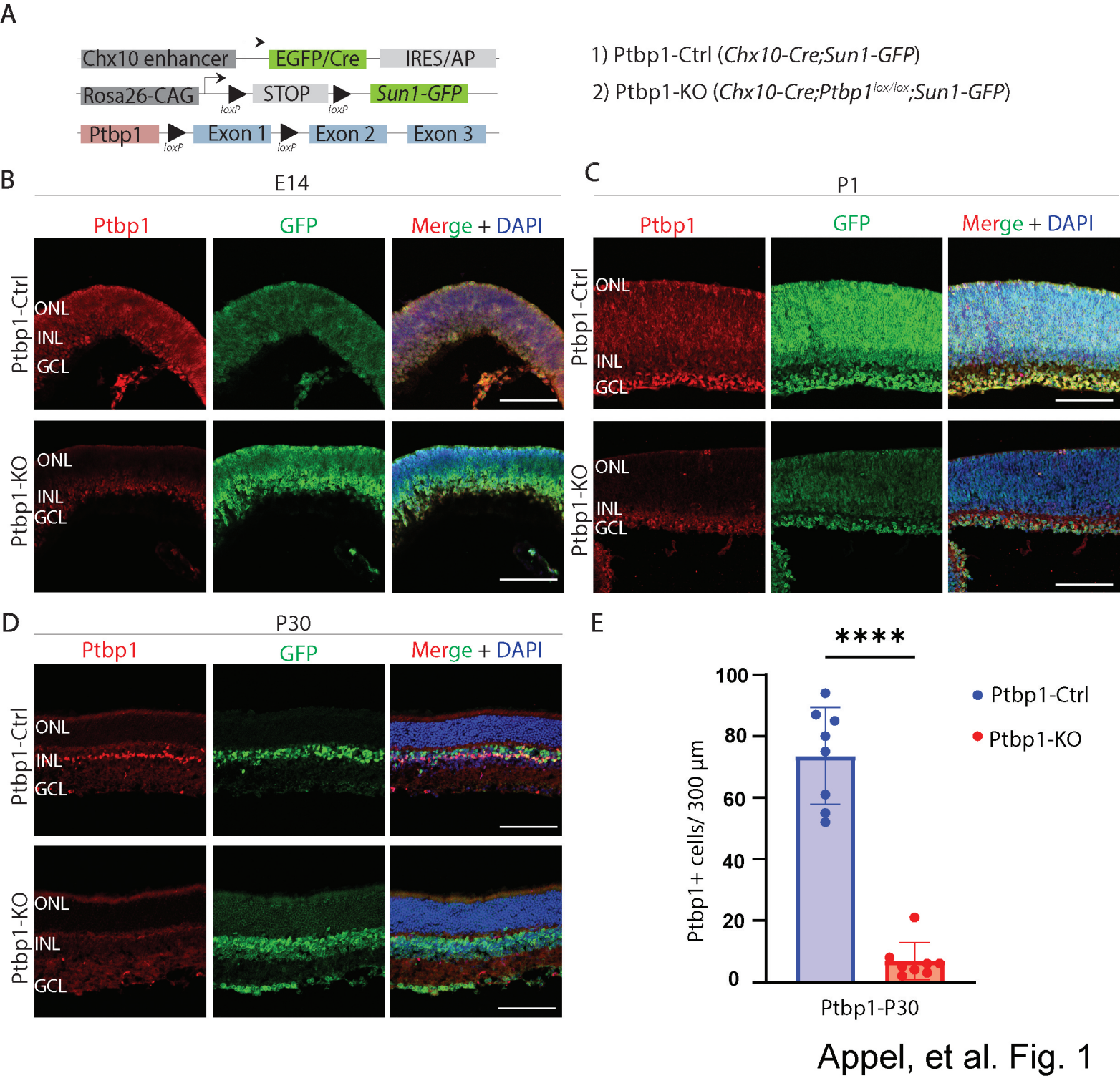
A
Chx10 enhancer
EGFP/Cre
IRES/AP
Rosa26-CAG
STOP
Sun1-GFP
loxP
loxP
Ptbp1
Exon 1
Exon 2
Exon 3
loxP
loxP
1) Ptbp1-Ctrl (Chx10-Cre;Sun1-GFP)
2) Ptbp1-KO (Chx10-Cre;Ptbp1lox/lox;Sun1-GFP)
B
E14
Ptbp1
GFP
Merge + DAPI
Ptbp1-Ctrl
Ptbp1-KO
ONL
INL
GCL
C
P1
D
P30
E
****
Ptbp1+ cells/ 300 µm
100
80
60
40
20
0
Ptbp1-Ctrl
Ptbp1-KO
Ptbp1-P30
Appel, et al. Fig. 1

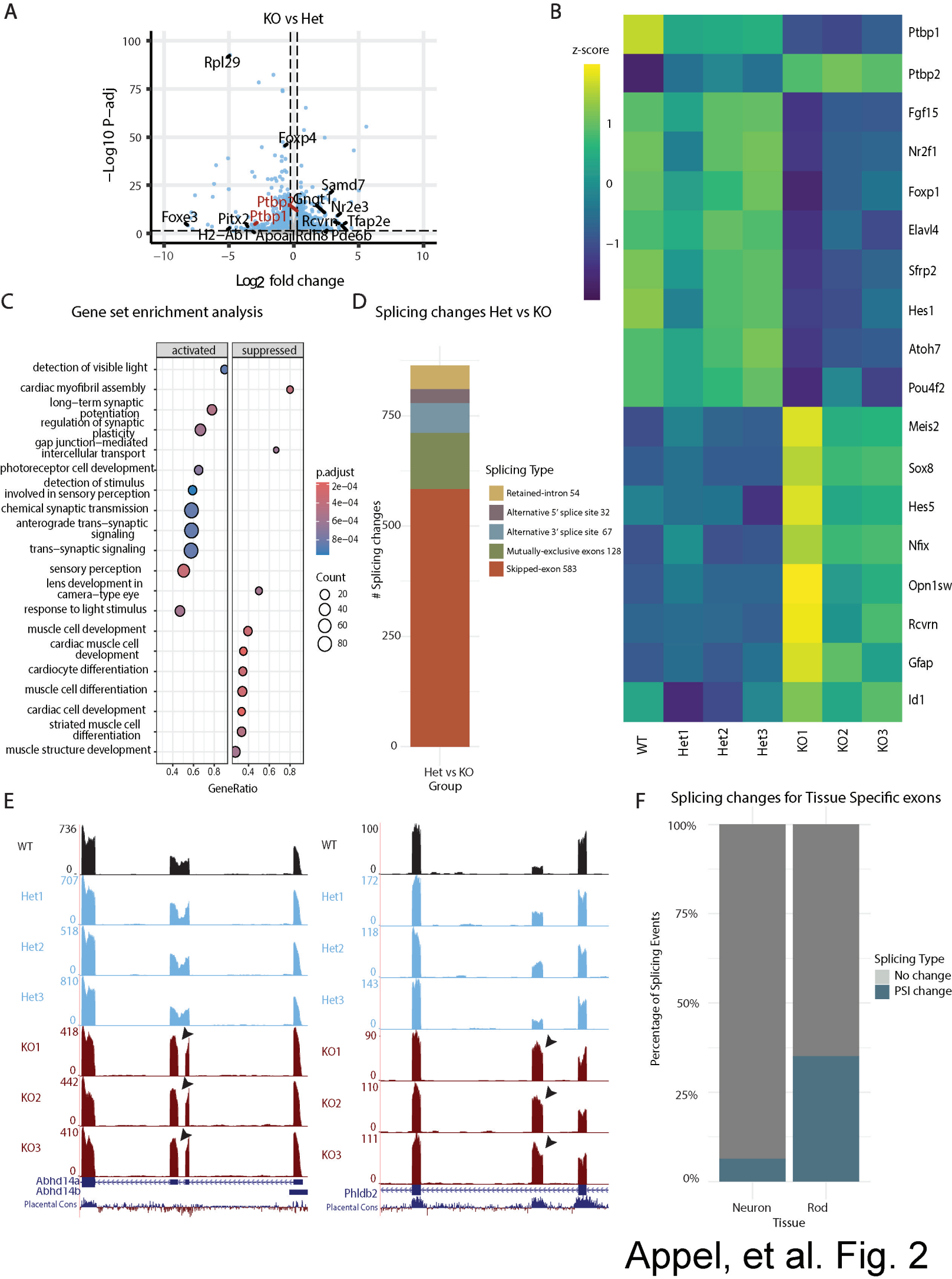

Appel, et al. Fig. 2

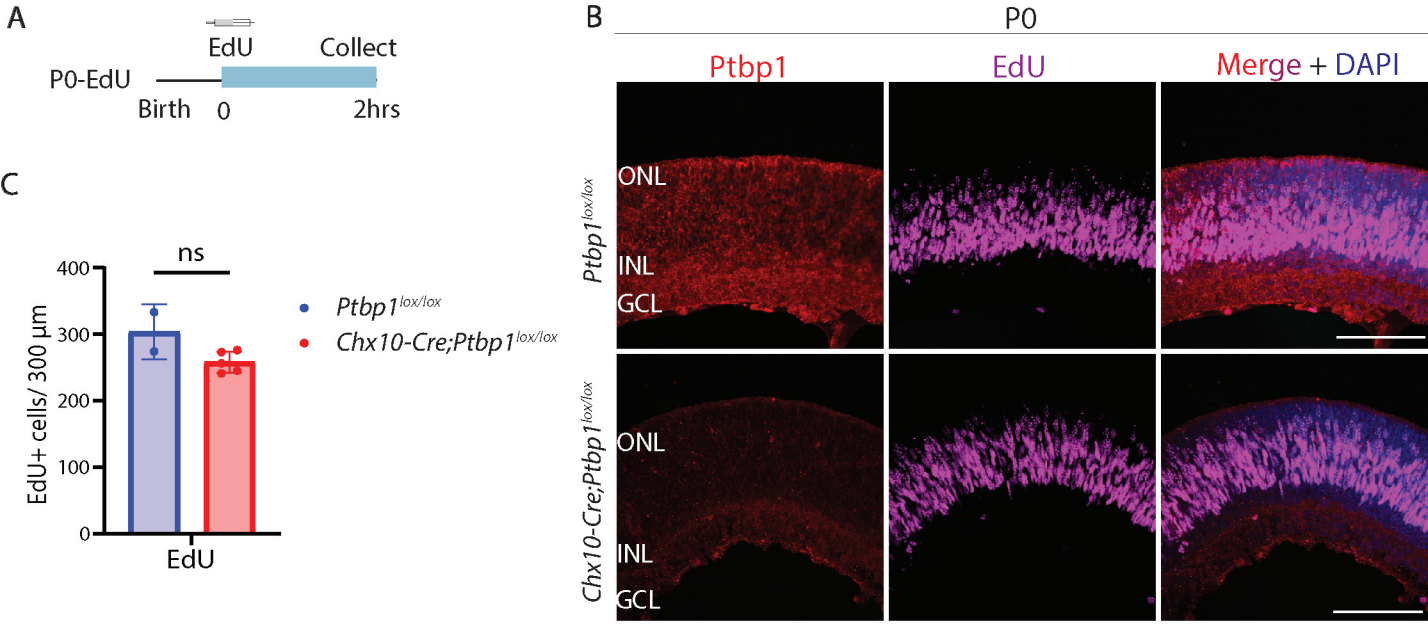

Appel, et al. Fig. 3

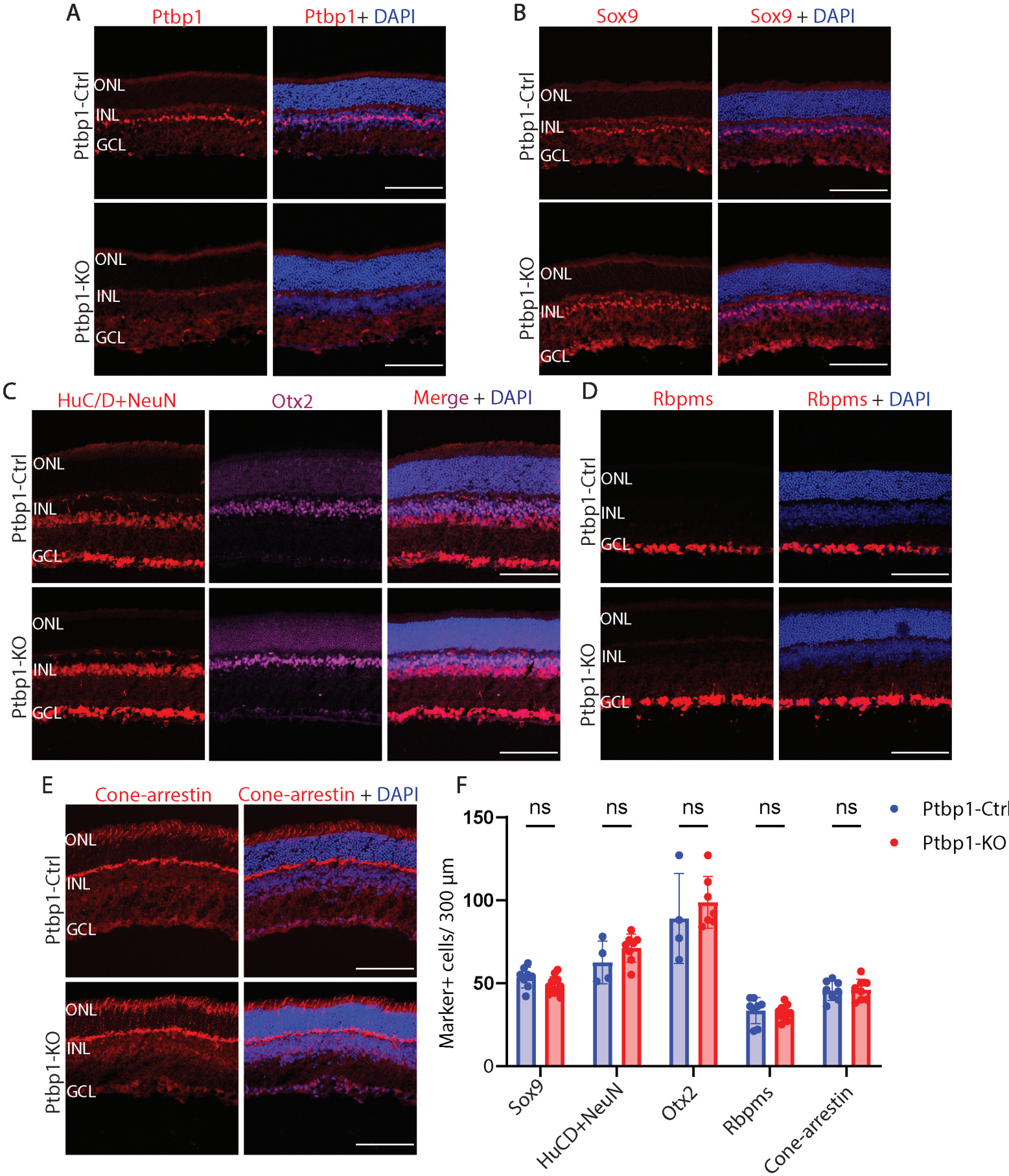

Appel, et al. Fig. 4

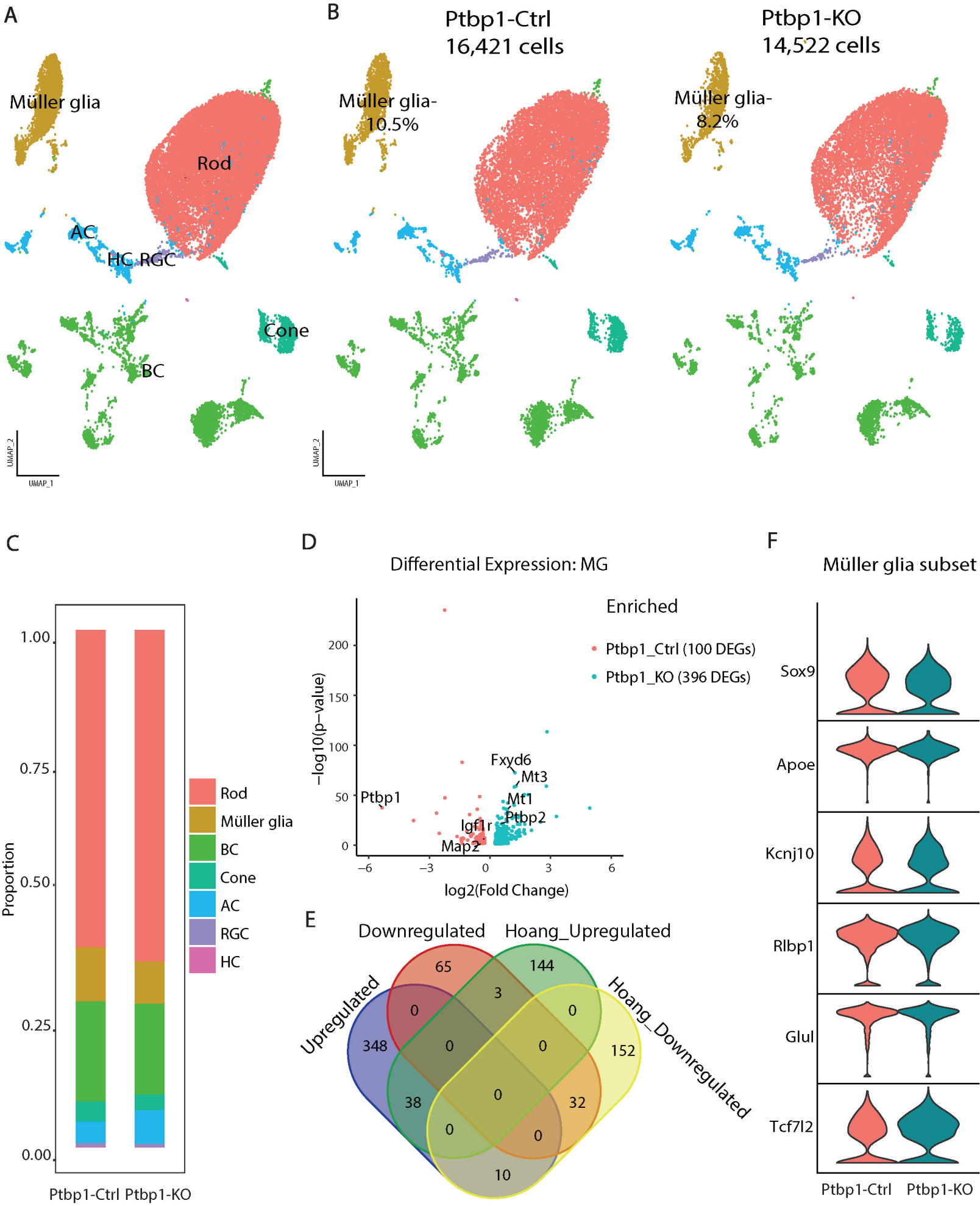

Appel, et al. Fig. 5

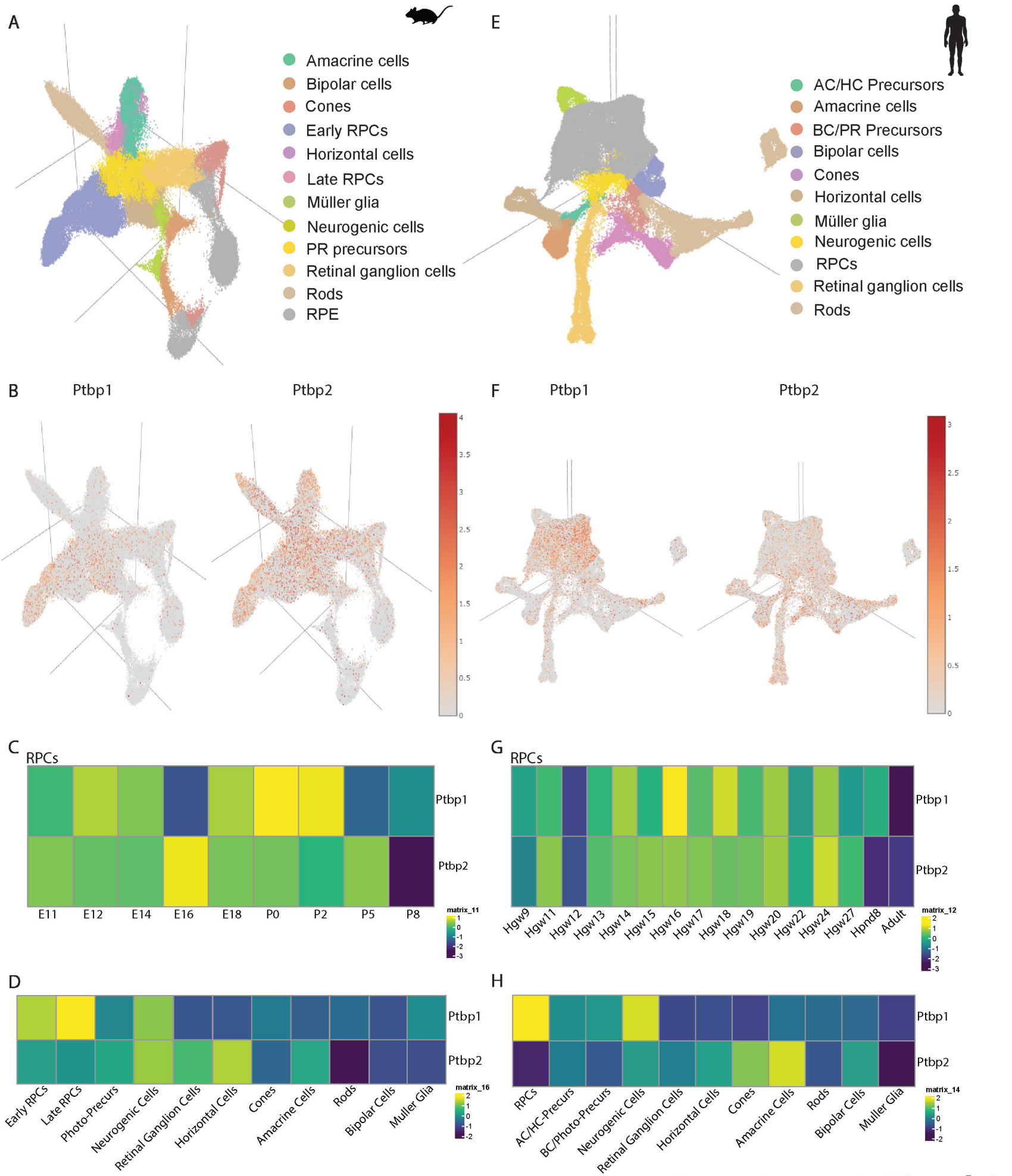

Appel, et al. Fig. S1

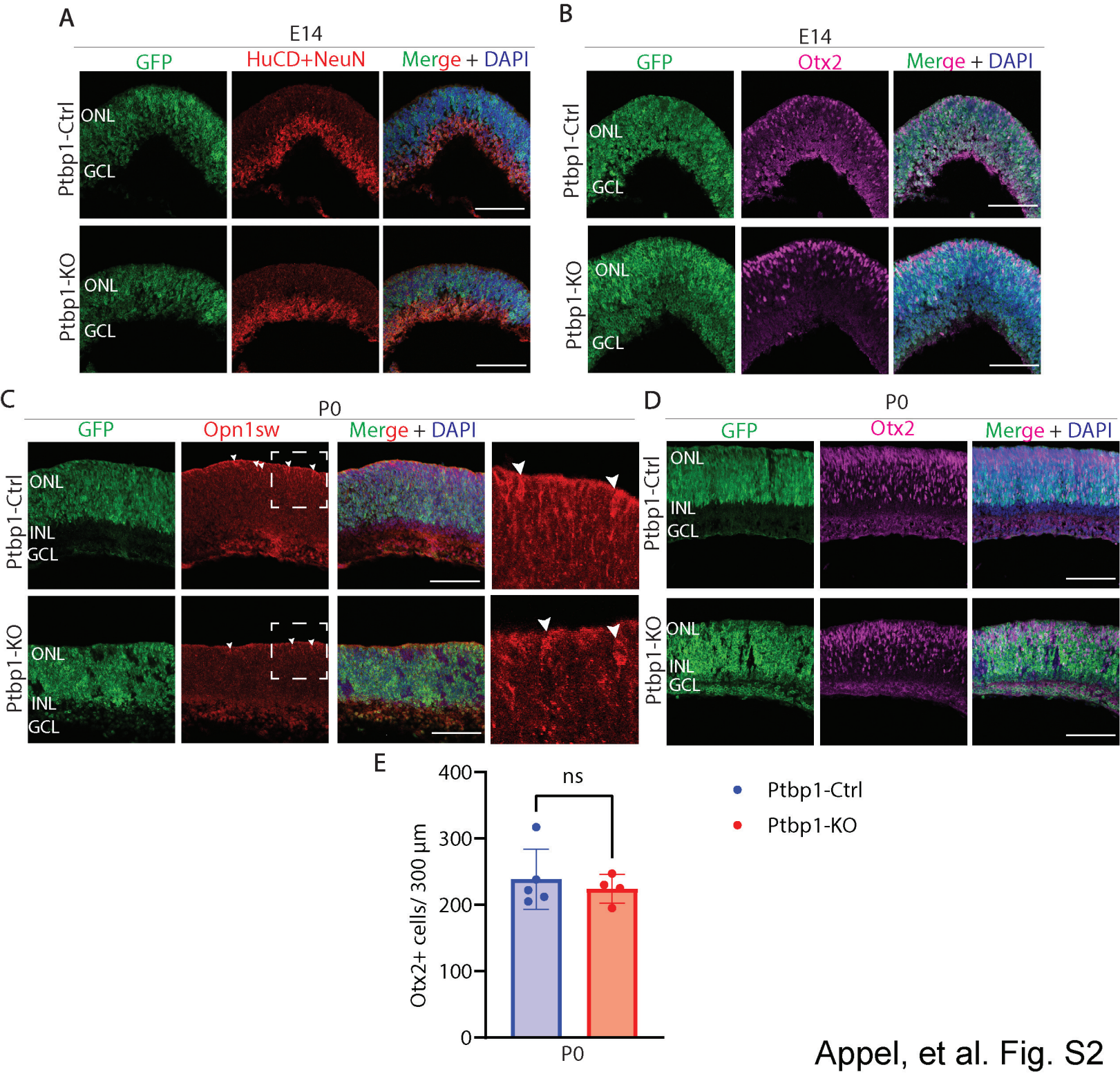

Appel, et al. Fig. S2

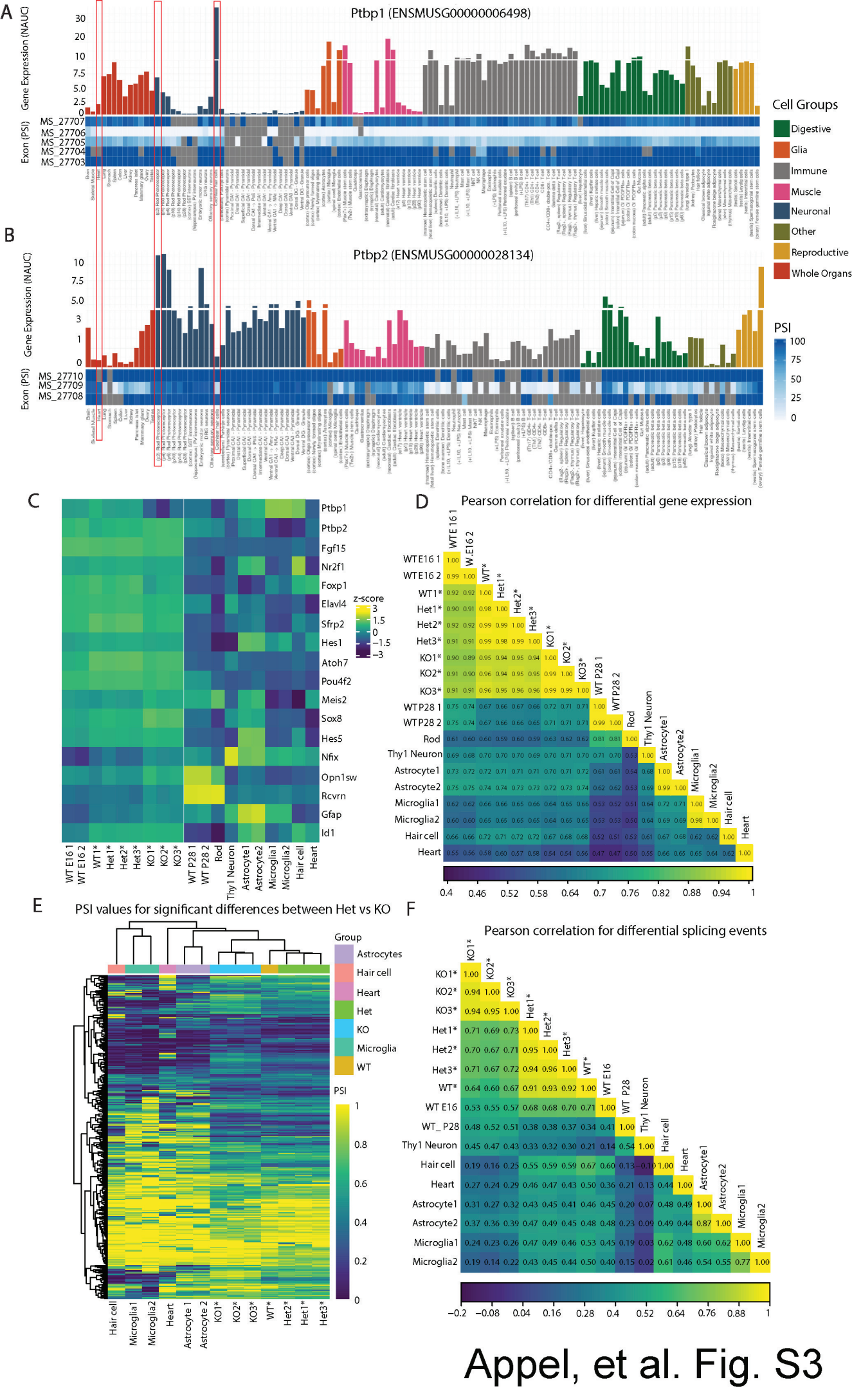

Appel, et al. Fig. S3

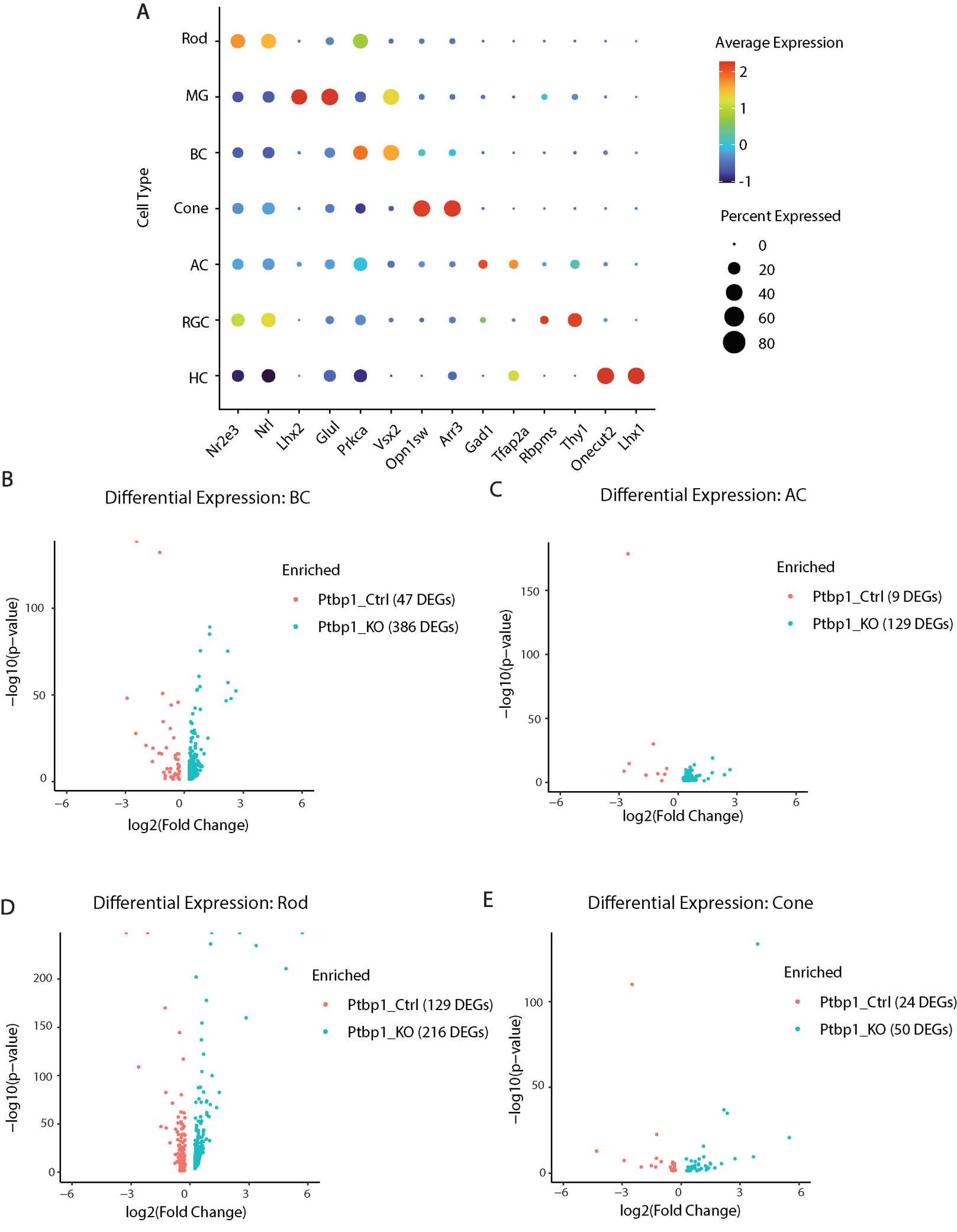

Appel, et al. Fig. S4